High electrical conductance enhancement in Au-nanoparticle decorated sparse single-wall carbon nanotube networks.

McAndrew, CF; Baxendale, M

High Electrical Conductance Enhancement in Au-Nanoparticle Decorated Sparse Single-Wall Carbon Nanotube Networks

*C. F. McAndrew and M. Baxendale**

School of Physics and Astronomy, Queen Mary University of London, Mile End Road, London, E14NS

*Corresponding author email: m.baxendale@qmul.ac.uk

ABSTRACT

We report high electrical conductivity enhancement in sparse single-walled carbon nanotube networks by decoration with Au nanoparticles. The optimised hybrid network exhibited a sheet resistance of 650 Ω/sq: 1/1500 of the resistance of the host undecorated network, with a negligible optical transmission penalty (>90% transmittance at 550 nm wavelength). The electrical transport at room temperature in host and decorated networks was dominated by 2-dimensional variable range hopping. The high conductance enhancement was due to positive charge transfer from the decorating Au nanoparticles in intimate contact with the host network causing a Fermi energy shift into the high density of states at a van Hove singularity and enhanced electron delocalisation relative to the host network which beneficially modifies the hopping parameters in such a way that the network behaves as an integral whole. The effect is most pronounced when the nanoparticle diameter is comparable to the electron mean free path in the bulk material at room temperature and there is minimum nanoparticle agglomeration. For higher than optimal values of nanoparticles per unit area or nanoparticle diameter, the conductivity enhancement is countered by metallic inclusions in the current pathways that are of higher resistance than the VRH-controlled elements.

1. INTRODUCTION

Individual single-walled carbon nanotubes (SWNTs) have desirable electrical, optical, thermal, and mechanical properties that suggest they are ideal elements for flexible transparent conducting networks with indium-doped tin oxide (ITO)-matching electrical and optical performance [1-3]. An

ideal SWNT network will have individual metallic SWNTs as the electrically conducting element, have zero inter-tube contact resistance, and be relatively ordered to minimise adverse electrical transport effects. The on- and off-tube optical transmission penalties for achieving the target sheet resistance of <100 Ω/sq must be minimised to achieve the target optical transmission of 90 % at 550 nm wavelength. Furthermore, the network must be chemically pristine to minimise device degradation and have a comparable work function and surface roughness to ITO films.

Actual SWNT networks are non-ideal since individual SWNTs of both semiconducting and metallic conduction types are produced by conventional syntheses, and some impurities can escape (or be introduced by) purification and filtration. The basic element is invariably a bundle rather than an individual SWNT and the use of ultrasonication to de-bundle in solution causes defectiveness and shortening [4]. Consequently there are large energy barriers at metal-semiconductor interfaces and disorder is introduced by the impurities and processing. Therefore, both the electrical transport within the bundle and the inter-bundle contact resistance has greatest influence on the electrical transport within the network as a whole [5, 6]. Solution processing typically requires the use of surfactants which can adversely impact on inter-tube resistance.

Handling in air also results in significant modification of electrical conductivity through exposure to oxygen and atmospheric humidity [7, 8] through donor- or acceptor-like charge transfer from weakly absorbed species which affects the position of the Fermi energy and hence the conductivity of the network. The absorption of gaseous species on the surface or inside of a nanotube bundle is stronger than that on an individual SWNT but is reversible [8, 9]. Oxygen-exposed networks have p-type characteristics due to transfer of $0.1e^-$ in the charge transfer complex $C^{+\delta}$-$O_2^{-\delta}$ [7]; subsequent adsorption of an electron from donor-like molecules will induce an increase of the resistance and the interaction with acceptor-like molecules will lead to a decrease of the resistance. In air-exposed networks, water molecules are donor-like and serve to compensate the electron acceptor effect of oxygen content [8-

10]. Consequently, the gas exposure history of a nanotube networks plays a critical role in determining the value of room temperature sheet resistance.

Many attempts have been made to optimise the room temperature conductance of nanotube networks by the chemical doping and hybridization with a host network of guest components by various methods, including acid treatment [11, 12], decoration by metal nanoparticles [3, 13], production of conducting polymer composite films [14] and graphene-SWNT networks [15].

The electrical transport properties of SWNT networks have been successfully described by a multi-component model involving metallic conduction interrupted by thin tunnel barriers, backscattering by zone-boundary phonons, fluctuation-assisted tunnelling, and variable-range hopping (VRH); the latter being tunnelling between localised states assisted by absorption of phonons. The relative contribution of each component is a function of network thickness: with VRH dominating the thinnest networks and metallic contribution increasing with thickness [16, 17]. The use of enriched metallic SWNT populations and purification through ultracentrifugation inevitably result in good electrical performance of SWNT networks through minimising both the semiconductor-metal junction density and disorder [7]. The high inter-bundle contact resistance is the main obstacle to enhancement of the electrical performance of SWNT networks [5, 6]. Inter-bundle contact resistances can be minimised by careful removal of residual surfactant [11].

Modification of the inter-bundle contacts via metal-nanoparticle decoration of the SWNT surface to obtain hybrid networks is gaining interest. This approach is driven by the observation of a factor of nine reduction of contact resistance between two individual SWNTs by placing a gold nanoparticle physically proximate to the junction and the prediction of resonant tunnelling through nanoparticle states [18, 19]. The electronic interaction between the nanotube network and the metal nanoparticles is of great interest due to the promise of selective gas sensing by exploiting differential analyte-nanoparticle reactivity and the consequent charge exchanges with the network [20], and useful plasmonic and thermoelectric benefits from such hybrid systems [21, 22]. However, the metal

nanoparticle-network interaction is poorly understood but the experimental data points to Au decoration of an individual SWNT resulting in electron transfer from the nanotube to the nanoparticle [13, 23, 24] and the formation of a potential barrier at the SWNT-metal interface where the barrier characteristics depend on the work function of the metal [25-27]. Computational predictions point to dramatic fluctuations in electronic density at the SWNT-metal interface being the origin of the potential barrier [28].

Many approaches for the preparation of such hybrid networks have been reported, including, physical evaporation of metal nanoparticles onto the SWNT network, nanoparticle attachment by chemical reaction with functionalised SWNTs, and electroless nanoparticle deposition methods [24, 29-33]. The room temperature sheet resistance of the resultant hybrid networks has been reported to be both increased [34, 35] and decreased [29] relative to the un-decorated SWNT network. The impact of nanoparticle decoration on the underlying electrical conduction mechanism of the host network is seldom elucidated beyond evocation of improved contact area between the elements of the network, general doping effects from SWNT nanoparticle bridging materials [36], work function increase through the doping effect of charge transfer from the nanoparticle [13], and disorder introduced by the processing [37].

The best enhancement of electrical conductivity reported to date is a 1/25 reduction of room temperature sheet resistance of a few-walled carbon nanotube network by Pd-nanoparticle decoration with an optical transmittance of 81.65% below the target figure of 90% at 550 nm wavelength [13]. The barrier to progress is largely conceptual: the room temperature sheet resistance is not a useful figure of merit since it embraces the many physical variables contained within the multiple component electrical conduction mechanism. A much better approach would be to drive optimisation by knowledge of the impact of nanoparticle decoration on each component of electrical conduction. Obtaining this knowledge is made difficult by the complex intra- and inter-bundle current pathways.

Here we present a systematic study of electrical transport in sparse SWNT networks decorated with Au nanoparticles relative to that of the host network. Sparse host networks were selected because the electrical transport was dominated by a single component, namely VRH. DFT calculations indicate that O_2 dissociation at the Au nanoparticle surface is energetically unfavourable, therefore, the expectation was of reinforcement of the p-type character of undecorated networks (due to handling in air) by Au nanoparticle decoration (due to the Fermi energy shift caused by electron transfer from the SWNTs to the Au nanoparticle) with no additional C-O charge transfer complexes on the surface of the nanoparticle [28]. We investigate electrical transport as a function of nanoparticle diameter and coverage using an electroless and a spraying method of nanoparticle decoration. We found that a 1/1500 reduction in room temperature sheet resistance of the host network can be achieved by optimised Au nanoparticle decoration through beneficial modification of the VRH transport caused by the Fermi energy shift, while maintaining over 90% optical transmittance at 550 nm wavelength.

2. EXPERIMENTAL

2.1. Host SWNT Network Preparation

Glass substrates, dimensions 20 mm × 20 mm, were cleaned by sonication in a solution of industrial detergent for 15 minutes followed by a further 15-minute sonication in isopropyl alcohol (Sigma-Aldrich, >99.7% purity) before drying under a nitrogen flow.

As-purchased SWNT powder (Unidym, diameter 0.8 -1.2 nm, length 100-1000 nm, <85% purity) was dispersed in 1:7 vol. solution of n-butylamine: tetrahydrofuran (both: Sigma Aldrich, >99% purity) then ultrasonicated (Sonics Ultrasonic Processor Model GE750 with CV 33 Probe, 750 W) for 1.5 hours using a 2 s-on, 3 s-off cycle at 450 W with the solution stood in an ice bath. The solution was sprayed with an Airbrush Pro series airbrush (model BD-133A) onto the substrates placed on a hotplate held at 379 K. The SWNT solution was sprayed onto each substrate through a 10 mm × 10 mm shadow mask. The dimensions of the showdown mask were chosen to be less than those of the substrate in order to define the active area and minimise edge conduction effects. The airbrush was cleaned thoroughly with ultrapure water after every 5 ml of solution had been sprayed to minimise the

corrosive effects of the solution on the airbrush and prevent blockage formation. The substrate-supported SWNT networks were then vacuum annealed for 1.5 hours at 400 K to remove residual solvent. This procedure was found to greatly improve the optical transparency and electrical conductivity of the networks relative to films deposited at room temperature without the annealing process. The room temperature conductance of the networks when exposed to the atmosphere varied from day to day by circa 10% due to physisorption of atmospheric dopants. When measured under vacuum, however, the sheet conductance was constant over a period of months.

2.2. Preparation of hybrid networks

We have applied two methodologies in order to independently investigate the effect that both Au nanoparticle diameter and nanoparticle number per unit area has on the electrical conduction mechanism of decorated sparse SWNT networks.

2.2.1. Preparation of hybrid networks: electroless method

Formation of Au nanoparticles on the host SWNT networks was achieved by the electroless reduction of Au cations by a redox reaction between Au^{3+} and the SWNT network. Chloroauric acid, $HAuCl_4{:}3H_2O$ (Sigma Aldrich, > 99% purity) was dissolved in 50% ethanol (Sigma Aldrich, 98% purity) to produce a 1mM solution. The substrate-supported SWNT networks were immersed in the solution for varying time periods. The network was then removed from the solution and rinsed in ultrapure water (PURELAB Prima DV35 system) before drying in nitrogen. The resultant hybrid networks were finally vacuum annealed for 1.5 hours at 400 K. The thus produced hybrid networks are free of degradations originating from acid dopants as evidenced by the time constant for current stabilisation which is sensitive to ionic mobility of residual acid molecules. The room temperature sheet resistance of the hybrid networks was stable over a timescale of months.

2.2.2. Preparation of hybrid networks: spraying method

As-purchased aqueous Au nanoparticle-containing colloidal solution (BBY international) was sprayed using a BD-133A airbrush with the host SWNT networks placed on a hotplate at 400 K. A sequence of 1 second spraying time followed by a 10 second delay was found to be the best strategy for

production of optically uniform networks. The resultant hybrid networks were finally vacuum annealed for 1.5 hours at 400K. The additional annealing process was found to have no significant effect on SWNT networks sprayed under the same conditions with only deionised water and those not subjected to a spray coating.

2.3. Characterisation

Four-probe electrical conductance measurements were performed under a vacuum of 10^{-6} mbar in Cryogenic 3165 Measurement System connected to a Keithley 4200 SCS source-measure unit with a pulsed-mode current of duration of 0.1 s. Electrical contact was made by a pressure contact at the corners of the active area. The initial resistance typically decreased by 5% and reached a steady-state after a few minutes due to outgassing of weakly chemisorbed dopants introduced by handling in air. The temperature of the system was controlled by a Lakeshore 340 system. The sample was left to equilibrate overnight at the base temperature.

The optical transmittance of each network was measured using a Hitachi U-3000 UV-vis spectrometer in high resolution mode in the wavelength range 400-800 nm.

Analysis of the morphology *i.e.* nanoparticle diameter and, nanoparticles per unit area, for both the host and decorated networks was carried out by visual inspection of SEM micrographs obtained using an FEI Inspect-F scanning electron microscope.

3. RESULTS AND DISCUSSION

The host sparse SWNT networks were deposited on glass substrates using a spraying method. The influence of surfactant on the host SWNT networks was minimised by using a volatile 1:7 volume mixture of n-butylamine: tetrahydrofuran as dispersant and solvent together with a post-deposition annealing process [38]. The resultant sparse networks comprised well-defined SWNT bundles of diameter 30±10 nm mainly confined to the plane of the substrate covering about 65% of the glass

surface, figure. 1. All electrical transport measurements were performed in equilibrium conditions under vacuum following an out-gassing procedure to minimise the role of weakly chemisorbed species introduced by handling in air. The method reproducibly resulted in a room temperature sheet resistance of R_s~1 MΩ/sq (conductance, G~ 1 μS/sq) with an active area of 10 mm × 10 mm for many tens of samples.

In agreement with a previous report, the temperature-dependant electrical transport measurements revealed a dominant VRH mechanism in the range T=4-225 K with a divergence in the range T=225-300 K, figure. 2 [38]. This divergence has the form of an additional thermally activated component,

$$G(T) = G_0 \exp\left(-\left(\frac{T_0}{T}\right)^{\gamma}\right) + G_a \exp\left(-\frac{E_a}{k_B T}\right), \quad (1)$$

where the first term is the Mott hopping formula with γ=1/(d+1) and d is the dimensionality of the hopping (i.e. d=1, 2 or 3) and the pre-exponential factor, G_0, and T_0 are constants [21]. The second term in Eqn. (1) is the thermally activated component, where E_a in the thermal activation energy, k_B is the Boltzmann constant, and G_a is a constant. The origin of this term is the presence of Schottky-like potential barriers at metallic-semiconductor junctions within current-carrying pathways [34].

We found there to be no significant contribution from fluctuation-assisted tunnelling. However, this does not exclude the possibility of metallic inclusions in non-metallic current pathways, only that this has negligible effect on the temperature dependence of electrical conductance [17].

We minimized the sum of the squares of the differences between the $G(T)$ data points in the range T=4-225 K and the function A.exp(−B/$T^{1/C}$) with A, B, and C taken as three independent parameters. From fits to transport data from tens of samples we obtained C=3 which suggest 2-dimensional VRH (i.e. a single inter-bundle hopping system within the plane of the network), B= T_0≈3.25 × 10^4 K, and A= G_0≈ 100 μS/sq. According to the Mott model for 2-dimensional VRH,

$$G_0 \sim \left(\frac{1}{L_{\mathrm{loc}}}\right)\left(\frac{T_0}{T}\right)^{0.35}, \quad (2)$$

and

$$T_0 = \frac{3}{k_{\mathrm{B}} N(E_{\mathrm{F}}) L_{\mathrm{loc}}^2}, \quad (3)$$

where L_{loc} is the localisation length, $N(E_{\mathrm{F}})$ is the density of states at the Fermi energy, and k_{B} is the Boltzmann constant [39]. The temperature dependence of G_0 was neglected in the data fitting procedure since the variation produced by the first exponent in Eqn.(1) dominates that of the pre-exponential factor. The uncertainty in the values of the extracted parameters for all experimental data sets were typically less than 10% with the exception of those for G_{a}, which were typically less than 35%.

The functional form of the divergence was found to be in agreement with the second term in Eqn.(1); the extracted value of $E_{\mathrm{a}} \approx 330$ meV was found to be close to the expected range of Schottky barrier heights at junctions between individual metallic and semiconducting nanotubes, namely 190–290 meV [41]. The fractional contribution to the total conductance at 290 K from the activated term at was estimated to be 8% using the value $G_{\mathrm{a}} \approx 0.4$ mS/sq and E_{a} extracted from the fitting process.

The effect of Au nanoparticle decoration on the electrical transport of host network as a function of nanoparticle diameter for an almost constant nanoparticle number per unit area was investigated using an electroless reduction process for nanoparticle decoration. The host networks were immersed in chloroauric acid for varying time periods before a rinsing process to remove acidic dopants. SEM micrographs reveal the formation of Au nanoparticles with a narrow distribution of diameters randomly distributed on the host SWNT network, figure 3. The narrow size distribution for a given immersion time is consistent with an initial seeding process followed by an increase in diameter with

increasing immersion time [13]. An approximate nanoparticle number per unit area of 50 μm^{-2} was confirmed by direct observation.

The immersion times are plotted against conductance of the networks measured after extraction from the solution, rinsing, and drying, figure 4. This showed an initial steep increase to reach a maximum after ~20 minutes immersion then a decrease with immersion time, figure 4. This trend is similar to that observed for electroless Au-decoration of few-walled carbon nanotube networks [29]. The mean diameter of the deposited nanoparticles was estimated from direct observation (SEM). The error on diameters obtained from the SEM micrographs was typically 5% and the full-width-half-maximum dispersion in nanoparticle diameter was <20%. The mean bundle diameter and junction density of the decorated network were comparable to those of the host network. The mean nanoparticle diameter that produced the maximum conductance enhancement was 47 nm.

Au nanoparticles in aqueous suspension were sprayed onto host networks for various exposure (deposition) times and plotted against conductance as a function of nanoparticle diameter in figure 5. The general trend for all three nanoparticle diameters, 2 nm, 10 nm, and 40 nm, is for a rapid increase in conductance with deposition time followed by a gentle decrease back to the initial values (or slightly less than the initial conductance in the case of the 40 nm diameter nanoparticle). The trends are most pronounced for the 40 nm diameter nanoparticle decorated films. The minimum sheet resistance was achieved was 650 Ω/sq: 1/1500 of that of the undecorated host network.

Inspection of the SEM micrographs for short- and long-exposure time for the 40 nm diameter nanoparticle-decorated networks revealed differing patterns of decoration. Essentially, the distribution in the short-exposure time is dominated by individual nanoparticles predominately located at the network junctions whereas the long-exposure distribution includes both individual nanoparticles in intimate contact with the host network and small agglomerations apparently templated by the underlying network (figure 6). For Au-nanoparticle coverage of $>400/\mu m^2$, the agglomerations become extensive and close-packed, figure 7.

Temperature-dependant electrical transport measurements were carried out to investigate the effect of nanoparticle diameter (at a near constant nanoparticle number per unit area). Networks decorated with nanoparticle diameters of 47 nm and 473 nm revealed the same dominant two-component variation as observed in the host networks but with some metallic departure from (2-dimensional) VRH at low temperature for the larger nanoparticle decoration, figure 8. The parameter extracted from the fitting of the data to Eqn.(1) are summarised together with those for the host networks (i.e., 0 immersion time) in Table 1

Table1. Diameter dependence of electrical transport parameters for host networks decorated by the electroless method.

Immersion time (min)	Mean diameter (nm)	G(290 K) (μS/sq)	G_0 (μS/sq)	T_0 (K)	G_a (μS/sq)	E_a (eV)
0	-	1	106	32535	42400	0.33
20	47	20	100	945	97	0.17
120	473	3.45	23	2000	7.31	0.11

The twenty-fold increase in G(290 K) relative to the host network for the 47 nm diameter nanoparticle decoration is clearly entirely due to the thirty-fold reduction in T_0 (since G_0 remained almost identical to that for the host network, and, using the extracted values of G_a and E_a, the calculated fractional contribution of the activated term to G(290 K) is negligible). Within the Mott hopping description, enhancement of the electron localisation length and/or the density of states at the Fermi energy are the factors that underpin the decrease in T_0, Eqn. (2).

A ten-fold increase in the diameter of the decorating nanoparticle to 473 nm results in a value of G(290 K) comparable to that of the host network but with G_0 reduced by a factor of five and T_0 by a factor of fifteen; also, the activated term is reduced to 2% of G(290 K). The low-temperature metallic

behaviour is manifest as a departure from VRH for T<125 K, figure 8. The nanoparticle diameter is three times greater than the intimate contact diameter, which is ~150 nm in this case (assuming a uniform distribution of seeding sites), so some contribution from all-metallic pathways can be expected to contribute to the total conductance.

Since, via Eqns. 2, 3, G_0 is proportional to T_0, the G_0 value for the 473 nm diameter nanoparticle decorated network must embrace a metallic term due to a significant contribution from metallic inclusions in the VRH network relative to the 47 nm diameter decorated network. G_0 can be viewed as the conductance of the network at high temperature, *i.e.* a measure of the intrinsic conductance of the network in the absence of significant energy barriers to electrical conduction. The temperature variation introduced by the metallic inclusions in the VRH network is expected to be that of a Bloch–Grüneisen-type power-law term for sheet resistance, $\sim T^n$ Ω/sq, where n=5 for electron-phonon interactions and n=2 for electron-electron interactions. The presence of significant metallic inclusions in the VRH pathways is, therefore, manifest as an effective negative offset to the G_0 value of the host network if the sum of the resistances of the metallic inclusions is higher than that of the VRH components of the pathway. This is manifested as an increase in T_0 but a decrease in G_0 as the nanoparticle diameter is increased from 47 nm to 473 nm, Table 1.

When considering the sources of this metallic component of conductance, there are two primary diameter-dependant effects at play. These are: i) the particle diameter at which, for a given number per unit area, the nanoparticles are in intimate contact and form a continuous metallic pathway larger than an individual nanoparticle, and ii) the diameter that is equal to electron mean free path within the individual nanoparticle. The electron mean free path in bulk Au is approximately 50 nm [42]. Therefore, metallic conduction within an individual nanoparticle is a rational explanation for the decrease in conductance with nanoparticle diameter in the range 50 nm – 150 nm. Metallic conduction pathways through multiple nanoparticles can be expected for diameters greater than ~150 nm.

From the extracted values of G_a and E_a we conclude there is no significant contribution to G(290 K) from the activated term, the second term in Eqn.1, for both the 47 nm and the 473 nm nanoparticle diameter decorated films. The diminution in this term occurs by an apparent lowering of both G_a and E_a. The lowering of E_a is consistent with modification of metal-semiconductor interfacial energy barriers through displacement of E_F toward the valence band in a p-type system, i.e. the host network. The lowering of G_a is consistent with the formation of a depletion region in those bundles in intimate contact with an Au nanoparticle, which results in an obstacle for hole transport and reduces hole mobility. This is consistent with observations on the scale of individual SWNTs intimately coupled to Au clusters in the gas sensing literature [25, 28].

In summary, the conclusions drawn from the data in figure 4. are: i) the rapid increase in conductance with particle diameter is due to enhancement of either of both electron delocalisation and the density of states at the Fermi energy, *i.e.* a decrease in the T_0 parameter relative to that of the host network, ii) for diameters >50 nm, the decrease in conduction is due to metallic conduction within an individual nanoparticle or multiple nanoparticles, iii) the inter-nanoparticle electronic transport is metallic and the intra-metallic island electron transport is by a 2-dimensional VRH, and iv) nanoparticles in intimate contact with the bundles of the host network are acceptor-like and possibly introduce significant depletion regions.

Temperature-dependant electrical transport measurements were performed on the 40 nm diameter nanoparticle-decorated networks and the results fitted to Eqn.1. The extracted parameters are summarised in Table 2.

Table 2. 40 nm-diameter nanoparticle coverage dependence of electrical transport parameters for host networks decorated by the spraying method.

Exposure time (s)	Nanoparticles (μm^{-2})	G(290 K) (μS/sq)	G_0 (μS/sq)	T_0 (K)	G_a (μS/sq)	E_a (eV)

0	0	1	106	32535	42400	0.33
6	5	11.5	18	341	66	0.14
8	8	1530	3400	153	-	-
60	100	3.43	7.31	209	5.8	0.09
100	170	1.9	5.7	903	48	0.11
180	343	0.9	4.46	1710	99	0.17

The networks with exposure times of 8 s (8 nanoparticles/μm^2 randomly dispersed, maximum conductance enhancement) and 180 s (343 nanoparticles/μm^2 agglomerated, conductance comparable to that of the host network) revealed both to be dominated by 2-dimensional VRH at room temperature, figures 9, 10. However, while the former is entirely VRH for the full range of temperature, the latter showed an additional metallic behaviour at low temperature (as observed for the 473 nm diameter nanoparticle-decorated networks produced by the electroless method, figure 8), see figure 10. The functional form of the resistance of this additional term was found to vary as T^5 indicating 3-dimensional Bloch–Grüneisen-type metallic conduction dominated by electron–phonon interactions. In the case of the agglomerated nanoparticle network, the calculated activated term is 5% of the total conductance at room temperature whereas there is zero contribution in the case of the optimally decorated network.

By consideration of the trends in G_0 and T_0 in Table 2, it is clear that for densities of ≥10 nanoparticles/μm^2, the decrease in G(290 K) is mainly due to enhancement of the metallic inclusions in VRH pathways. The VRH parameters for the optimally decorated network follow the expected trend in G_0 and T_0 relative to the host network indicating a much lower metallic component than the other nanoparticle densities.

The absence of a significant activated term for the optimally decorated film also indicates that the system is a single VRH network. The trends in G_a and E_a are indicative of a rapid reduction of both

the energy barrier and G_a with nanoparticle decoration for densities <10/μm^2 and a gradual reversal of this these trends for <10/μm^2. A logical explanation for the trends in the activated term as the nanoparticle density tends to 10/μm^2 would be a diminution of the mean energy barrier at a metal-semiconductor junction as the interfacial energy barrier is lowered by positive charge transfer to the bundles at intimate nanoparticle-bundle junctions. The reversal of this trend for densities >10/μm^2 is likely to be a due to compensating nanoparticle-nanoparticle charge transfer with the onset of agglomeration or n-type doping originating from the water in which the nanoparticles are suspended during spraying. The variation of G_a with nanoparticle density follows the inverse of G(290 K) so is likely to be an indication of the number of pathways (*i.e.* the fractional contribution to the total conductance). The zero metal-semiconductor energy barrier for the optimally decorated network is synonymous with a greatly enhanced density of states at the Fermi energy in the semiconductor regions in a p-type system as E_F coincides with a van Hove singularity, resulting in the observed all-VRH system with enhanced G_0 (through Eqn.2) and diminished T_0 (through Eqn.3) relative to the host network.

4. CONCLUSION

In conclusion, the resistance of the host sparse SWNT networks was lowered by a factor of 1500 by decoration with 40 nm diameter Au-nanoparticles with coverage of ~10 nanoparticles/μm^2. The electrical transport at room temperature in host and decorated networks was dominated by 2-dimensional Mott VRH. The high conductance enhancement was due to positive charge transfer from the decorating Au-nanoparticles in intimate contact with the host network causing a Fermi energy shift into the high density of states at a van Hove singularity and enhanced electron delocalisation relative to the host network which beneficially modifies the VRH parameters in such a way that the network behaves as an integral whole. The effect is most pronounced when the nanoparticle diameter is comparable to the electron mean free path in the bulk material, ~50 nm in this case, and there is minimum nanoparticle agglomeration. For higher than optimal values of nanoparticles per unit area or nanoparticle diameter, the conductivity enhancement is countered by metallic inclusions in the current pathways that are of higher resistance than the VRH-controlled elements.

Acknowledgement

The authors thank the Engineering and Physical Science Research Council for funding through the Imperial College London/ Queen Mary University of London Plastic Electronics Doctoral Training Centre.

References

1. Grüner G, 2006 Carbon Nanotube Films for Transparent and Plastic Electronics *J. Mater. Chem.* **16** 3533-3539.
2. Niu C M, Carbon Nanotube Transparent Conducting Films 2011 *MRS Bulletin* **36** 766-773.
3. Yang S B, Kong B S, Jung D H, Baek Y K, Han C S, Oh S K, Jung H T, 2011 Recent Advances in Hybrids of Carbon Nanotube Network Films and Nanomaterials for their Potential Applications as Transparent Conducting Films *Nanoscale* **3** 1361-1373.
4. Vichchulada P, Cauble M A, Abdi E A, Obi E I, Zhang Q, Lay M D 2010 Sonication Power for Length Control of Single-Walled Carbon Nanotubes in Aqueous Suspensions used for 2-Dimensional Network Formation *J. Phys. Chem. C* **114** 12490–12495.
5. Hecht D, Hu L, Grüner G 2006 Conductivity Scaling with Bundle Length and Diameter in Single Walled Carbon Nanotube Networks *Appl. Phys. Lett* **89** 133112.
6. Garrett M P, Ivanov I N, Gerhardt R A, Puretzky A A, Geohegan D B 2010 Separation of Junction and Bundle Resistance in Single Wall Carbon Nanotube Percolation Networks by Impedance Spectroscopy *Appl. Phys. Lett*. **97** 163105.
7. Collins P G, Bradley B, Ishigami M, Zettl A 2000 Extreme Oxygen Sensitivity of Electronic Properties of Carbon Nanotubes *Science.* **287**, 1801-1804.
8. Romero H E, Sumanasekera G U, Kishore S, Eklund P C, 2004 Effects of Adsorption of Alcohol and Water on the Electrical Transport of Carbon Nanotube Bundles *J. Phys. Condens. Matter*. **16** 1939-1949.
9. Zhao J, Buldum A, Han J, Lu J P, 2002 Gas Molecule Adsorption in Carbon Nanotubes and Nanotube Bundles *Nanotechnology.* **13** 195-200.
10. Zahab A, Spina L, Poncharal P, Marliere C 2000 Water-Vapor Effect on the Electrical Conductivity of a Single-Walled Carbon Nanotube Mat. *Phys. Rev. B.* **62** 10000-10003.
11. Geng H-Z, Kim K K, So K P, Lee Y S, Chang Y, Lee Y H J 2007 Effect of Acid Treatment on Carbon Nanotube-Based Flexible Transparent Conducting Films *Am. Chem. Soc*. **129** 7758-7759.

12. Parekh B B, Fanchini G, Eda G, and Chhowalla M 2007 Improved Conductivity of Transparent Single-Wall Carbon Nanotube Thin Films via Stable Post Deposition Functionalization *Appl. Phys. Lett*. **90** 121913.
13. Li Y A, Tai N H, Chen S K, Tsai T Y 2011 Enhancing the Electrical Conductivity of Carbon-Nanotube-Based Transparent Conductive Films using Functionalized Few-Walled Carbon Nanotubes Decorated with Palladium Nanoparticles as Fillers *ACS Nano*. **5** 6500-6506.
14. Yun H, Han J-H, Kim S 2012 Fabrication of Conductive and Transparent Single-Walled Carbon Nanotube Films with PEDOT *Polymer Journal.* **44** 1238-1243.
15. Tung V C, Chen L-M, Allen M J, Wassei J K, Nelson K, Kaner R B, Yang Y 2009 Low-Temperature Solution Processing of Graphene ─ Carbon Nanotube Hybrid Materials for High-Performance Transparent Conductors *Nano Lett*. **9** 1949-1955.
16. Kaiser A B, Skákalová V, Roth S 2008 Modelling Conduction in Carbon Nanotube Networks with Different Thickness, Chemical Treatment and Irradiation *Physica E* **40** 2311-2318.
17. Skákalová V, Kaiser A B, Woo Y-S, Roth S 2006 Electronic Transport in Carbon Nanotubes: From Individual Nanotubes to Thin and Thick Networks *Phys. Rev. B* **74** 085403.
18. Smorodin T, Beierlein U, Kotthaus J P 2005 Contacting Gold Nanoparticles with Carbon Nanotubes by Self-Assembly *IOP. Nanotechnol*. **16** 1123.
19. Khoo K H, Chelikowsky J R 2009 Electron Transport Across Carbon Nanotube Junctions Decorated with Au Nanoparticles: Density Functional Calculations *Phys. Rev. B,* **79** 205422.
20. Zanolli Z, Leghrib R, Felten A, Pireaux J-J, Liobet E, Charlier J-C 2011 Gas Sensing with Au-Decorated Carbon Nanotubes *ACSNano.* **5** 4592-4599.
21. Chen Y C, Young R J, Macpherson J V, Wilson N R 2007 Single-Walled Carbon Nanotube Networks Decorated with Silver Nanoparticles: A Novel Graded SERS Substrate *J. Phys. Chem. C.* **111** 16167-16173.
22. Ryu Y, Freeman D, Choongho Y 2011 High Electrical Conductivity and n-Type Thermopower from Double-/Single-Wall Carbon Nanotubes by Manipulating Charge Interactions Between Nanotubes and Organic/Inorganic Nanomaterials *Carbon*. **49** 4745-4751.

23. Yang S B, Kong B-S, Kim D-W, Baek Y-K, Jung H-T. 2010 Effect of Au Doping and Defects on the Conductivity of Single-Walled Carbon Nanotube Transparent Conducting Network Films *J. Phys. Chem. C.* **114** 9296–9300.
24. Kim Y T, Mitani T 2006 Surface Thiolation of Carbon Nanotubes as Supports: A Promising Route for the High Dispersion of Pt Nanoparticles for Electrocatalysts *J. Catal*. **238** 394-401.
25. Kauffman D R, Star A 2007 Chemically Induced Potential Barriers at the Carbon Nanotube-Metal Nanoparticle Interface *Nano Lett*. **7** 1863-1868.
26. Mubeen S, Lim J-H, Srirangarajam A, Mulchandani A. Deshusses, M A, Myung N V 2011 Gas Sensing Mechanism of Gold Nanoparticles Decorated Single-Walled Carbon Nanotubes *Electroanalysis*, **23** 2687-2692.
27. Seo S M, Kang T J, Cheon J H, Lim J, Chung I Y, Kim Y H, Y J Park 2011 Statistical Property of the Effect of Au Nanoparticle Decoration on the Carbon Nanotube Network *Appl. Phys. Lett*. **98** 143106.
28. Kauffman D R, Sorescu D C, Schofield D P, Allen B L, Jordan K D, Star A 2010 Understanding the Sensor Response of Metal-Decorated Carbon Nanotubes *Nano Lett.***10** 958-963.
29. Kong B S, Jung D H, Oh S K, Han C S, Jung H T 2007 Single-Walled Carbon Nanotube Gold Nanohybrids: Application in Highly Effective Transparent and Conductive Films *J. Phys. Chem. C*. **111** 8377-8382.
30. Jiang H J, Zhao Y, Yang H, Akins D L 2009 Synthesis and Electrochemical Properties of Single-Walled Carbon Nanotube–Gold Nanoparticle Composites *Materials Chemistry and Physics.* **114** 879-883.
31. Wang D, Li Z C, Chen L W 2006 Templated Synthesis of Single-Walled Carbon Nanotube and Metal Nanoparticle Assemblies in Solution *J. Am. Chem. Soc*. **128** 15078.
32. Hrapovic S, Liu Y, Male K B, Luong J H T 2004 Electrochemical Biosensing Platforms using Platinum Nanoparticles and Carbon Nanotubes *Anal. Chem*. **76** 1083-1088.
33. Smorodin T, Beierlein U, Kotthaus J P 2005 Contacting Gold Nanoparticles with Carbon Nanotubes by Self-Assembly *IOP. Nanotechnol*. **16** 1123.

34. Songmee N, Daothong S, Singjai P J 2008 Negative Temperature Coefficient of Single-Walled Carbon Nanotube-Gold Nanoparticle Hybrid Structures *Nanosci. Nanotechnol*. **8** 2522-2525.

35. Yang S B, Kong B S, Kim D W, Jung H T 2010 Comparison of the Stability of Surface-Modified SWNTs and DWNTs Network Films *J. Phys. Chem. C*. **114** 4395-4398.

36. Guo D-J, Li H-L 2004 Electrochemical Synthesis of Pd Nanoparticles on Functional MWNT Surfaces *Electrochem. Commun*. **6** 999-1003.

37. Oh S-D, So B-K, Choi S-H, Gopalan A, Lee K-P, Yoon K R, Choi I S 2005 Dispersing of Ag, Pd, and Pt–Ru Alloy Nanoparticles on Single-Walled Carbon Nanotubes by γ-Irradiation *Mater. Lett*. **59** 1121-1124.

38. Ravi S, Kaiser A B, Bumby C W 2010 Improved Conduction in Transparent Single Walled Carbon Nanotube Networks Drop-Cast from Volatile Amine Dispersions *Chem. Phys. Lett*. **496** 80-85.

39. Mott N F, Davis E A 1979 Electron Processes in Non-Crystalline Materials, Clarendon Press, Oxford,; pp 32-36.

40. Topinka M A, Rowell M W, Goldhaber-Gordon D, McGehee M D, Hecht D S, Gruner G 2009 Charge Transport in Interpenetrating Networks of Semiconducting and Metallic Carbon Nanotubes *Nano Lett*. **9** 1866.

41. Fuhrer M S, Nygård J, Shih L, Forero M, Yoon Y-G, Mazzoni M S C, Choi H-J, Ihn J, Louie S G, Zettl A, McEuen P L 2000 Crossed Nanotube Junctions *Science*. **288** 494-497.

42. Link S, Burda C, Wang Z L, E-Sayed M A 1999 Electron Dynamics in Gold and Gold–Silver Alloy Nanoparticles: The Influence of a Nonequilibrium Electron Distribution and the Size Dependence of the Electron–Phonon Relaxation *J. Chem. Phys*. **111** 1255-1265.

Figures

Figure 1

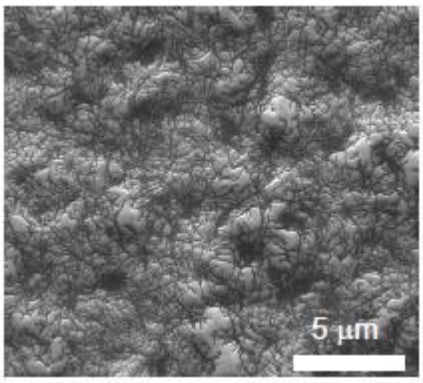

Scanning electron micrograph of a typical host network on a flat glass substrate. The apparent uneven surface morphology of the glass surface is an artefact caused by the difference between the high electrical conductivity of the network and the low value of that of the glass substrate.

Figure 2

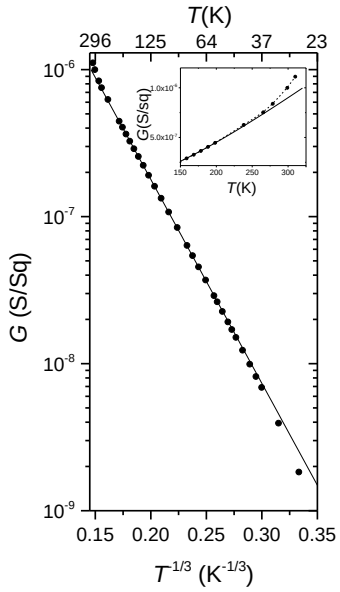

A typical temperature variation of conductance for a host network. The solid line is the 2-dimensional Mott VRH component (the first term in Eqn. (1)) extracted from the data fitting procedure. The inset shows the T>225 K departure from VRH; the dashed line is the fit to the activated term (second term in Eqn. (2)).

Figure 3

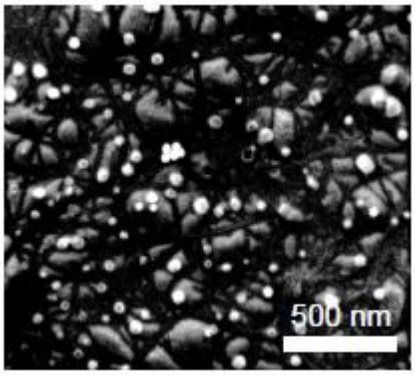

Scanning electron micrograph of a host network decorated with Au nanoparticles by the electroless method. The mean nanoparticle diameter is 47 nm.

Figure 4

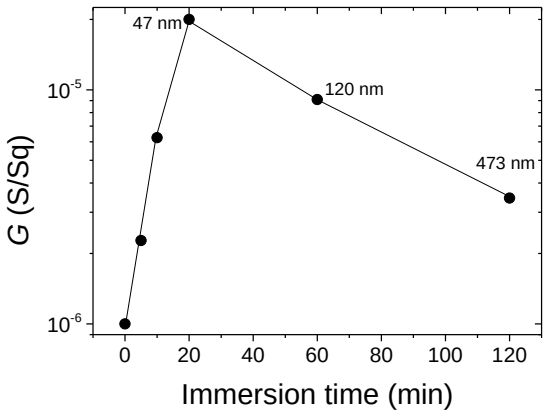

The conductance of Au-nanoparticle decorated networks prepared by the electroless method, measured after rinsing and drying, versus the immersion time.

Figure 5

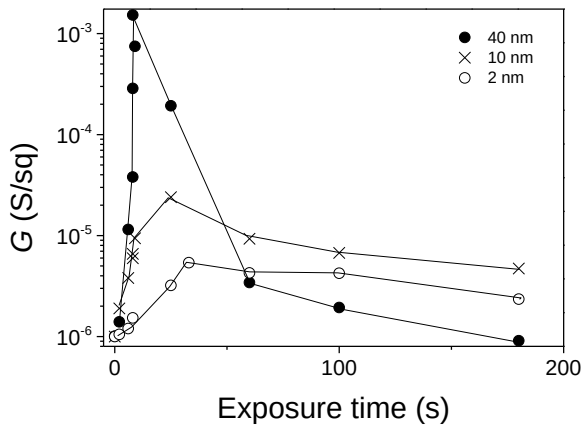

The conductance of Au-nanoparticle decorated networks prepared by the spraying method, measured after rinsing and drying, versus the exposure time as a function of nanoparticle diameter.

Figure 6

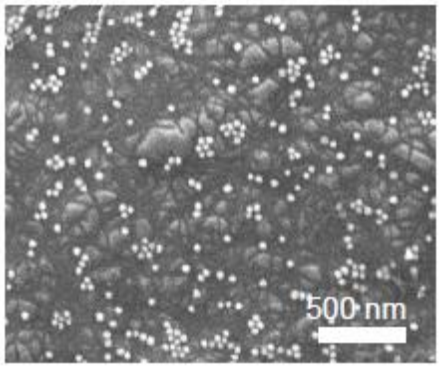

Scanning electron micrograph of host network decorated with 40 nm diameter Au nanoparticles by the spraying method. The number of nanoparticles per unit area is 100/μm^2 averaged over a 50 μm × 50 μm area.

Figure 7

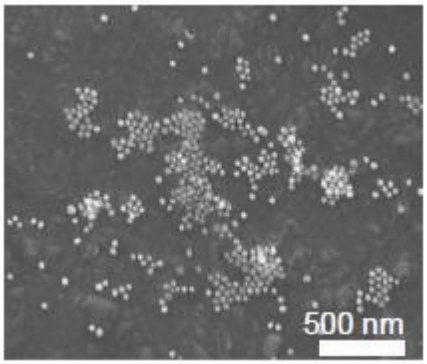

Scanning electron micrograph of host network decorated with 40 nm diameter Au nanoparticles by the spraying method. The number of nanoparticles per unit area is 170/μm^2 averaged over a 50 μm × 50 μm area.

Figure 8

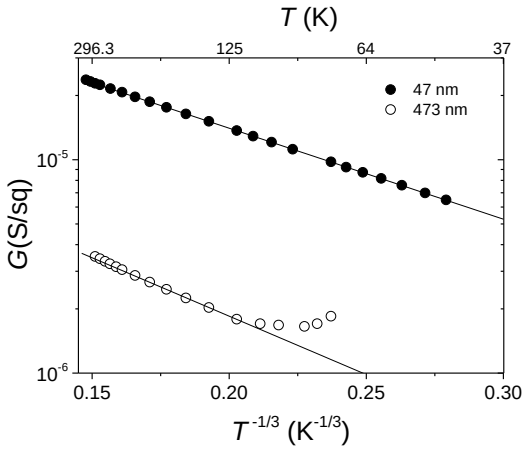

Typical temperature variation of conductance for networks decorated with Au nanoparticles by the electroless method. The mean nanoparticle diameter for the filled-circle data points is 47 nm and that for the open-circle points is 473 nm. The solid line is the 2-dimensional Mott VRH component extracted from the data fitting procedure.

Figure 9

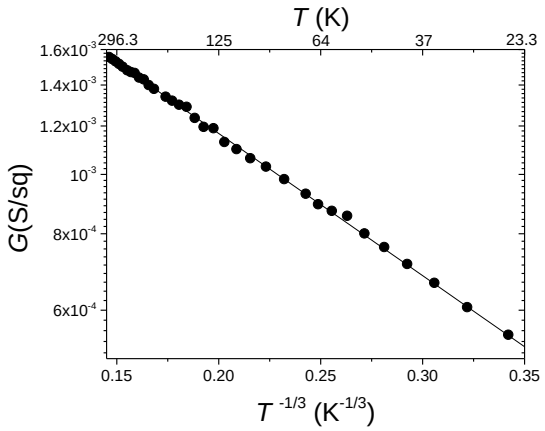

Typical temperature variation of conductance for networks decorated with 40 nm diameter Au nanoparticles by the spaying method with a coverage of 8 nanoparticles/μm^2. The solid line is the 2-dimensional Mott VRH component extracted from the data fitting procedure.

Figure 10

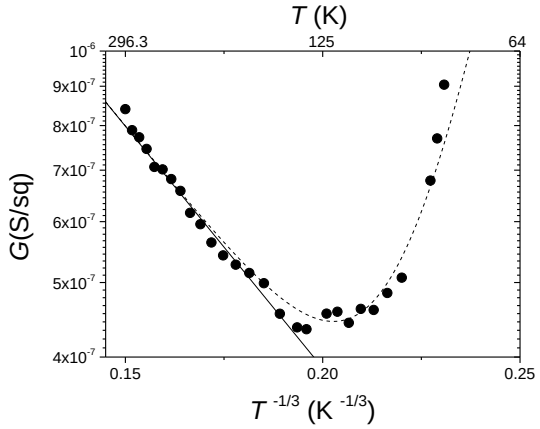

Typical temperature variation of conductance for networks decorated with 40 nm diameter Au nanoparticles by the spaying method with a coverage of 343 nanoparticles/μm^2. The solid line is the 2-dimensional Mott VRH component extracted from the data fitting procedure. The dashed line is an additional ~T^5 Bloch–Grüneisen-type metallic component.